Volume 1 | Number 1 | Jan 2013 | Pages 1–100

Journal of
Materials Chemistry B

Materials for biology and medicine
www.rsc.org/materialsB

ROYAL SOCIETY
OF CHEMISTRY

ROYAL SOCIETY
OF CHEMISTRY

www.rsc.org/materialsB

Iridium oxide nanoparticles induced dual catalytic/inhibition based detection of phenol and pesticide compounds

Carmen C. Mayorga-Martinez[a‡], Flavio Pino[a‡], Sevinc Kurbanoglu[a,b‡], Lourdes Rivas[a], Sibel A. Ozkan[b], Arben Merkoçi[a,c*]

Environmental pollution control technology has a great demand for detection systems, particularly for pesticides and phenolic compounds. Moreover, analytical systems are highly requested for the dual detection of different pollutants using the same platform. In that direction, a new, reliable, easy to use and disposable biosensor for the detection of catechol and chlorpyrifos is proposed. The designed biosensor with synergic properties between the high conductivity of iridium oxide nanoparticles, low-cost screen printed electrodes and the efficiency of tyrosinase shows broad linearity ranges for catechol and chlorpyrifos detection. Using this biosensor, very low limits of detection for catechol (0.08 μM) and chlorpyrifos (0.003 μM) are observed and recoveries of spiked tap and river water samples have also been studied showing very good recoveries.

Introduction

The detection of polluting compounds is a major concern for health and environmental government institutions. Among all pollutant compounds, organophosphate pesticide (OP) and phenol compounds are the most toxic and dangerous ones for human being [1, 2]. It is well known that pesticide and phenol compounds possess high acute toxicity. For instance, chlorpyrifos (CPF), one of the most widely used OP, interferes with brain development in part due to alterations in the activity of transcription factors involved in the basal machinery of cell replication and differentiation [3] and phenol is potential human carcinogen and is of considerable health concern, even at low levels [4].

Pesticides are extensively used in farming and domestic purposes [5]. Phenol compounds have limited use in industry process for different purposes [6]. In fact, everyday those compounds are easily released in different water systems affecting the ecosystem.

Nowadays, the detection of pesticides and phenol compounds is performed using large and expensive automated analysers such as liquid chromatography coupled with mass spectroscopy [7, 8] and high pressure liquid chromatography [9,10]. These techniques reach low limit of detection and high reproducibility but involve extraction of large volumes of water, require extensive purification and expensive equipment. Therefore, there is a high demand to obtain simple analytical devices and related nanomaterials for the detection of the mentioned hazard compounds in environment and health related samples. The main prospective of the future detection systems are to be cheap, reliable, easy to be used and disposable. At the same time, it would be necessary to have devices that can detect different family of pollutants.

Currently different approaches for the detection of pesticides, including immunoassay [11] and enzymatic activity [12] have been developed. Enzymatic biosensors are the most reliable for this type of analysis due to their simplicity, efficiency and their easy usage. In fact, numerous biosensors about using inhibition-based enzymatic systems in particularly those based on the inhibition of AChE [13, 14] have been reported. Furthermore, tyrosinase (Tyr) was used for phenolic compound detection and based on the inhibition of this enzyme few pesticide detections have been reported [15, 16]

The advantage of the Tyr based electrochemical biosensor is its achieved selectivity due to the fact that the effect of interfering species such as other electroactive compounds is low given its low working potential (-0.2V or less) [17-19] in comparison to acetyl cholinesterase (AChE) and free mediators based biosystems that mostly use to work at 0.6 V [20].

Meanwhile, the request for a disposable analytical platform could be reached through the use of micro-transducers like screen printed carbon electrode (SPCE). In fact in the last twenty years, the application of these devices for in-situ and user-friendly measurements is significantly increased. The key factor in an enzymatic micro-device platform is the immobilization procedure of the enzyme. This process is usually performed in different ways; adsorption, entrapment and cross–linking are the most reported. The main-objective of the enzyme immobilization alternatives has always been the increase of the biosensor stability and its reproducibility being fouling of the working electrode surface the most important drawback to overcome [21, 22].

The explosion in nanomaterials research, especially nanoparticles, has influence also the research, in the field of enzymatic biosensor [23, 24]. The connection of enzymatic systems with nanoparticles has a high impact on improving the performance of the platform used for detection of toxic compounds. This is due to the unique, chemical, physical and electronic properties at nanoscale effect possessed by nanoparticles (normally in the range of 1 – 100 nm) [25, 26]. Iridium oxide (IrOx) films have been used in biosensors as electrodes (enzymes can be immobilized) due to their high conductivity [27]. Furthermore, IrOx nanoparticles, as new emerging metal nanoparticles, possess useful electronic and conductivity switching properties which make them highly attractive for biosensors development as well [28].

In the present study, an enzymatic biosensor for dual detection of two different pollutants, catechol (a phenol derivate) and chlorpyrifos (an organophosphate pesticide) is proposed. Such sensing is achieved through a SPCE modified with IrOx NPs and Tyrosinase. The proposed biosensor reports improvement in the limit of detection (0.08 μM) and sensitivity for catechol compared to previously reported biosensors. This biosensor shows also low limit of detection (0.003 μM) for CPF while being used in a tyrosinase inhibition mode operation. Finally the efficiency of this biosensor for real applications in CPF detection in river and tap water was also explored showing great possibilities for future application as a low cost platform for pesticide detection.

Experimental

Materials and apparatus

Electrochemical experiments were performed using an electrochemical analyzer Autolab 20 (Eco-Chemie, The Netherlands) which was connected to a personal computer using a software package GPS 4.9 (General Purpose Electrochemical System). Impedance measurements were performed by using an Autolab302 potentiostat/galvanostat/frequency-response analyzer PGST30, controlled by GPES/FRA Version 4.9. Scanning electrochemical microscopy (SEM) images were acquired using a Field Emission-Scanning Electron Microscopy (Merlin, Carl Zeiss) and Transmission electron microscope (TEM) images were taken with a JEM-2011(Jeol,Ltd., Japan). A thermoshaker TS1 (Biometra) was used to stir the samples during inhibition process operating at controlled temperature of 37.5 °C and 350 rpm of shaking. Homemade screen printed carbon electrodes (SPCEs), were used as the electrochemical transducer which are constituted by three electrodes in a single strip: carbon working electrode with diameter of 3 mm, Ag/AgCl reference electrode and carbon counter electrode.

Reagents and solutions

Tyrosinase from mushroom (≥1000 unit/mg), bovine serum albumin (BSA), glutaraldehyde (GA, 25%), chlorpyrifos and catechol were purchased from Sigma-Aldrich (St. Louis, MO). For the synthesis of iridium oxide nanoparticles, potassium hexachloroiridate-(IV), sodium hydrogencitrate, were purchased from Sigma-Aldrich (St. Louis, MO). Milli-Q water was obtained from purification system and all solutions were prepared with ultra-pure water from a Millipore-MilliQ system. All reagents and other inorganic chemicals were supplied by Sigma-Aldrich or Fluka, unless otherwise stated.

Synthesis of iridium oxide nanoparticles

Iridium oxide nanoparticles were prepared according to the previously reported procedure [29]. Potassium hexachloroiridate-(IV) 2.6×10^{-5} M solution was mixed with sodium hydrogencitrate 1.6×10^{-2} M solution. The pH of the red brown solution was adjusted to pH

7.5 with a 0.25 M NaOH solution and then refluxed in an oil bath with constant stirring for 30 min. As the mixture cooled to room temperature, the pH was again adjusted to 7.5 with a reflux for 30 min. This procedure was repeated until pH reached a constant value of 7.5. Finally the solution was refluxed 2 h more with oxygen bubbling. At the end of this step, a deep blue solution of IrOx nanoparticles was obtained. The solution was stocked in a glass-stoppered flask and at 4ºC when not in use.

Preparation and modification of Screen Printed Electrodes

Screen printing electrodes were fabricated by sequential deposition of a graphite ink, Ag/AgCl ink and insulating ink on a polyester substrate. The polyester substrate was dried at 120 °C for 45 min (graphite) and 30 min (Ag/AgCl and insulating) after the deposition of each layer. Before modification, SPCEs were activated at 3 µA for 120 sec in 0.1 M H_2SO_4. A 5µL solution of IrOx NPs suspension was dropped onto the working surface of SPCE. 0.25 % of gluteraldehyde (GA) was prepared in ultra-pure water and from this solution 5 µL was dropped onto the SPCE/IrOx surface. 2 µL of the solution of Tyr (1 mg/ 50 µL) in BSA 5% (1:1) was dropped onto SPCE/IrOx/GA surface. Tyr and BSA solution were prepared in 0.1 M phosphate buffer at pH 6.5. In between all steps, electrodes were allowed to be dried at 37.5 °C for 30 min.

Electrochemical measurements

The surface characterization of the modified electrodes was performed by electrochemical impedance spectroscopy (EIS) studies in 1mM $[Fe(CN)_6]^{3-/4-}$ with 0.1 M KCl as redox probe. A sinusoidal potential modulation of ± 50 mV amplitude in the 0.1 Hz to 100 kHz frequency range, with logarithmic scale of 10 points per decade, was superimposed onto the formal potential of the redox couple, $[Fe(CN)_6]^{3-/4-}$ (0.24 V vs Ag/AgCl). Nyquist diagrams were also recorded.

Chrono-amperometric measurements were conducted at -200 mV; magnetic stirrer was used to provide the convective transport in 10 mL of 0.1 M phosphate buffer with 0.1 M KCl. Electrochemical experiments were carried out at room temperature.

Results and discussion

Morphological studies.

Transmission electron microscopy (TEM) micrograph of IrOx NPs was performed to determine the sizes and homogeneity. Figure 1A displays the typical TEM image of the synthesized IrOx nanoparticles (12.5 ± 2.5 nm) (see inset in Fig. 1A). Although the dispersion of these nanoparticles was not homogenous in the solution, most of the formed IrOx NPs exhibited special shape. These nanoparticles seem to be cluster of other smaller nanoparticles with diameter around 1.5 ± 0.3 nm.

The XPS spectra of IrOx NPs (Figure S1) showed the shifting of the Ir $4f_{7/2}$ and $4f_{5/2}$ peaks to ~ 62.3 and ~ 65.1 eV, and an increase of the O 1s peak intensity at 531.6 eV (main peak) and 533.7 eV (small one) being these results in good agreement with the characteristics with high oxidation state 4^+ of iridium.

IrOx NPs were immobilized onto working electrode of SPCE, then glutaraldehyde (GA) was used as cross-linking agent followed by a modification with a solution composed of tyrosinase and BSA. The obtained biosensor was carefully characterized in each of the fabrication step by using optical and electrochemical methods. Figure 1B shows a scanning electron microscopy (SEM) image of SPCE (left image correspond to backscattered electrons mode). Figure 1C displays the distribution of the IrOx NPs onto the working electrode surface of the SPCE. IrOx NPs appear brighter in the obtained image (Figure 1C left), while the effect of glutaraldehyde as a binding matrix was more evident in normal mode (Figure 1C right). An enhancement of the contrast between objects of different chemical compositions using backscatter electrons mode is observed, since heavy elements backscatter electrons more strongly than light elements. Finally Figure 1D shows a good entrapment of the IrOx NPs, glutaraldehyde and Tyrosinase-BSA.

To study the surface features of the modified electrodes, electrochemical impedances spectroscopy was used. The EIS curve presented as Nyquist plot consists in two parts: one part is the semicircle section, located at higher frequencies corresponding to the electron transfer limited process. The second part, is relate to the electron-transfer resistance (Rct) and can be obtained by measuring its diameter. Another important part of Nyquist plot is the linear section, which brings the information related to the diffusion process held in solution and located at lower frequencies. The increase of

electron transference due to the presence of IrOx NPs layer was observed with the decreasing of Rct in the Nyquist plot (see Figure 1E). These improvements were due to the fact that IrOx is a metallic oxide known for its high conductivity that corresponds to high oxidation state (4^+) of iridium [27, 30]. Additionally, this nanostructured platform based in IrOx NPs has a high superficial area that contributes the conductivity improvement.

The adsorption of glutaraldehyde onto the IrOx (see Rct increase at Figure 1E) indicates the effect of glutaraldehyde as a good binding / entrapment matrix. Finally, when the solution composed of Tyr-BSA was introduced (adsorbed onto the electrode surface) an increasing of Rct as result of a successful immobilization of the enzyme could be observed (Fig. 1 E).

The SPCE/ IrOx/Tyr biosensor operation for the catechol detection was evaluated by chrono-amperometric responses for the different enzyme modified sensors upon successive addition of 5 µM catechol (Fig 2). This biosensor showed a higher current change in comparison to the SPCE/Tyr (Fig. 2A). The observed reduction of the current was attributed to the direct reduction of o-quinone to catechol, released from the enzyme-catalyzed reaction on the electrode surface (see Fig. 3A and B). Tyrosinase has oxidase activity for oxidation of catechol to o-quinone (see Figure 3B). At moderate negative potential the o-quinone product of phenol oxidation may be electrochemically reduced to catechol (Figure 2A). Oxidation by the enzyme followed by reduction at the electrode may result in cycling between the catechol and o-quinone [18].

Figure 2B shows a good selectivity of this biosensor toward catechol detection that is evident by the shown neglected responses toward interfering species. The chrono-amperometric responses toward aniline, benzaldehyde, benzylalcohol, Mg^{2+}, Ca^{2+} (each one in a concentration 10 times higher than phenol concentration) and Cu^{+2} (5 times higher than phenol concentration) were measured. The selected species for interference studies seem to be the ones usually present with the phenolic compounds in contaminated samples [18].

Analytical characterization of the biosensor

Chrono-amperometric response of the SPCE/IrOx/Tyr biosensor to successive additions of catechol solution (Figure 4A) is further evaluated under optimized experimental conditions (data not shown). The linear biosensor response within the range from 0.25 µM – 27.5µM catechol with r= 0.99 was

observed. The biosensor shows sensitive bioelectrocatalytic response, reaching about 95% of the steady-state current within 10s after each addition of catechol.

The typical calibration curves of the SPCE/IrOx/Tyr for catechol is showed in Figure 4B. Moreover, LOD and LOQ were calculated according to the 3 times s/m and 10 times s/m criterions, respectively, where 's' is the standard deviation of the peak currents of low concentration of the analyte (five runs) and 'm' is the slope of the related calibration graph [31-35]. SPCE/IrOx/Tyr biosensor shows LOD=0.08 µM and LOQ=0.24 µM for catechol. The results of triplicate sets indicated by error bars reveal the in-day repeatability (Figure 4B) of the measurements with a relative standard deviation (RSD) lower than 10%. Between day repeatability also obtained with a RSD value lower than 15%.

Pesticides are known to inhibit different enzymatic systems being tyrosinase one of these [15]. To evaluate pesticide inhibition activity onto the tyrosinase biosensor, the 'percentage inhibition' method was followed. The Tyr biosensor is immersed into a buffer solution under stirring condition and addition of catechol 5 µM was performed waiting until achieving a steady state current response.

The stationary state current after each addition (Iss) is related to the enzyme activity of the biosensor when the inhibitor is not present. After that the same biosensor is incubated during a fixed interval of time (30 min) with chlorpyrifos pesticide. The pesticide incubated biosensor was measured again after the addition of the same concentration of catechol (5 µM). Lower steady state-currents (Ip) were obtained due to the inhibition by pesticide. The Tyr biosensor inhibition percentage is calculated using the following equation:

$$I(\%) = \left[\frac{(I_{ss} - I_p)}{I_{ss}} \right] * 100 \qquad (1)$$

In order to optimize the testing variables for pesticide detection using tyrosinase inhibition, catechol concentration and incubation time were evaluated in presence of 0.1 µM chlorpyrifos. Figure 5A shows the optimum catechol concentration value to be used as working substrate for Tyr inhibition experiments. Herein different concentrations of catechol (1, 2 and 5 µM) were used, and the best inhibition response was found to be achieved for a 5 µM substrate solution. The incubation time was also evaluated (see Figure 5B) showing that when the incubation time increased the inhibition also

increased. A 30 min incubation time (under stirring condition at 37.5 ºC) was used for the following experiments.

Plots of the biosensor inhibition percentage as a function of pesticide concentration are shown in Figure 6A. The proposed biosensor provides linear range for chlorpyrifos concentration from 0.01 to 0.1 µM with a correlation coefficient of 0.99 with a LOD=0.003 µM and LOQ=0.010 µM. As the pesticide irreversibly inhibits the enzyme, a new biosensor has to be used for each point of the calibration after being exposed to the pesticide. The results indicated by error bars reveal the in-day repeatability (Figure 6A) of the measurements with a relative standard deviation (RSD) lower than 15%. Between days repeatability was also obtained with a RSD value lower than 15%. These biosensors for CFP detection present high analytical performances in term of sensitivity and LOD (Table 1 SI Section).

To further demonstrate the applicability of the proposed biosensor, recovery tests by adding chlorpyrifos 0.1 µM into river and tap water were also performed. The results are presented in Figure 6B. Recovery percentages of 113 % ± 3.6 and 90 % ± 9.6 for tap and river water respectively with RSD lower than 10% (n=3) were found. Recovery percentages were calculated using equation (2). This indicates that the proposed biosensor can be used for trace pesticide level detection in real samples. In addition it is possible to detect catechol and CPF using the same platform given the fact that the catechol detection is almost instantaneous (10 s response time) and CPF detection requires a longer response (30 min) (See figure 7). It also can be extended to other kind of enzymes and pollutants detection with interest for environmental monitoring.

$$recovery\ percentage = \left(\frac{[CPF]_{buffer}}{[CPF]_{real\ sample}} \right) *100 \quad (2)$$

Conclusions

An IrOx NPs based biosensing platform with effective tyrosinase immobilization properties and corresponding catalytic effect toward catechol is developed. Due to the high conductive and the surface active area of the IrOx NPs, the proposed biosensor displays dramatic improvements of the analytical performance in terms of a wider linear range of response along with a good LOD and

sensitivity for catechol detection. Moreover the chlorpyrifos pesticide is detected using the same biosensor through the enzyme inhibition mechanism. The LOD was found to be 0.003 μM which is lower than the maximum contaminant level recommended by the European Environment Bureau [36]. In addition to the analytical performance the use of this biosensor for chlorpyrifos detection has advantages in comparison to other ones reported before (Table 1, SI Section) due to the fact that it is related to a simple cost/efficient screen-printed carbon electrode. In addition it is possible to detect catechol and CPF using the same platform. A careful operation of this platform should be versatile and efficient enough for dual detection applications. This dual phenol/pesticide detection biosensing system can be extended to other enzymes and consequently to other pollutants combining direct (catalytic) and indirect (inhibition) detections in the same platform.

Acknowledgements

Notes and references

[a]Nanobioelectronics & Biosensors Group, ICN2- Institut Catala de Nanociencia i Nanotecnologia, Campus UAB, 08193, Bellaterra, Barcelona, Spain

[b]Ankara University, Faculty of Pharmacy, Department of Analytical Chemistry, 06100, Tandogan, Ankara, Turkey

[c]ICREA, Barcelona, Catalonia, Spain.

* E-mail: arben.merkoci@icn.cat

[‡]C. C. M.-M. , F. P. and S. K. contributed equally to this work.

Electronic Supplementary Information (ESI) available: [details of any supplementary information available should be included here]. See DOI: 10.1039/b000000x/

1 G. Aragay, F. Pino and A. Merkoçi. *Chem. Rev.,* 2012, **112**, 5317–5338.

2 C.W. Heath, *Cancer*, 1997, **80**, 1887-1888.

3 M. E. Ridanoa, A. C. Raccaa, J. Flores-Martína, S. A. Camolottoa, G. Magnarelli de Potasb, S. Genti-Raimondia and G. M. Panzetta-Dutaria, *Reprod. Toxicol.* 2012, **33** 331– 338.

4 Bódalo, E. Gómez, A. M. Hidalgo, M. Gómez, M.D. Murcia and I. López, *Desalination* 2009, **245**, 680–686.

5 S. Viswanathan, H. Radecka, J. Radecki, *Biosens. Bioelectron.* 2009, **24**, 2772-2777.

6 W. Zhonga, D. Wanga, X. Xua, *J. Hazard Mater.* 2012, **217**, 286– 292.

7 A.Vermeulen, K. Welvaert and J. Vercammen, *J Chromatogr. A,* 2005, **1071**, 41-46.

8 J. Gundel and J. Angerer, *J. Chromatogr. B*, 2000, **738**, 47-55.

9 J. Sherma, *Anal. Chem,* 1995, **65**, 40R-54R.

10 I. Valenzuela, R. Lorenzini, M. J. Redondo and G. Font, *J. Chromatogr. A* 1999, **839**, 101–107.

11 H. Wang, J. Wang, C. Timchalk and Y. H. Lin, *Anal. Chem.* 2008, **80**, 8477-8484.

12 D. Du, W. Chen, W. Zhang, D. Liu, H. Li and Y. Lin, *Biosens. Bioelectron*. 2010, **25**, 1370-1375.

13 J. Gong, Z. Guan and D. Song, *Biosens. Bioelectron,* 2013, **39**, 320-323.

14 F. Arduini, S. Guidone, A. Amine, G. Palleschi and D. J. Moscone *Sensor. Actuat. B-Chem* 2013, **179**, 201– 208

15 T. Liu, M. Xu, H. Yin, S. Ai, X. Qu, and S. Zong, *Microchim. Acta.* 2011, **175**, 129-135

16 S. Solé, A. Merkoçi, and S. Alegret, *Crit. Rev. Anal. Chem*, 2003, **33**, 89–126.

17 Y. D. Tanimoto de Albuquerque and L. F. Ferreira *Anal. Chim. Acta* 2006, **596**, 210-221.

18 C. C. Mayorga-Martinez, M. Cadevall, M. Guix, J. Ros, A. Merkoçi. *Biosens. Bioelectron,* 2013, **40**, 57–62.

19 B. Pérez-López and A. Merkoçi. *Adv. Funct. Mat.,* 2011, **21**, 255-260.

20 C. Zhai, X. Sun, W. Sao, Z. Gong, X. Wang, *Biosens. Bioelectron*. 2013, **42**, 124-130.

21 S. Andrescu, L. Barthelmebs, J. L. Marty, *Anal. Chim. Acta*; 2002, **464**,171-180.

22 J. P. Hart and S. A. Wring, *Trends Anal. Chem* 1997, **16**, 89-103.

23 L. Zamifir, L. Rotariu, C. Bala, *Biosens. Bioelectron*. 2011, **26**, 3692-3695.

24 Y. Lin, F. Lu, J. Wang, *Electroanalysis,* 2004, **16**, 145-149.

25 S. Taufik, N.A.T. Yusof, W. Tee, I. Ramli, *Int. J. Electrochem*. 2011, **6**, 1880–1891.

26 E. Katz and I. Willner, *Angew. Chem. Int. Ed.* 2004, **43**, 6042–6108.

27 C. C. Mayorga Martinez, R. E. Madrid and C. J. Felice, *Sensor. Actuat. B-Chem* 2008, **133**, 682–686.

28 J. Tang, D. Tang, R. Niessner, D. Knopp, *Anal Bioanal Chem*, 2011, **400**, 2041–2051.

29 T. Kuwabara, E. Tomita, S. Sakita, D. Hasegawa, K. Sone and M. Yagi, *J. Phys. Chem. C* 2008, **112**, 3774-3779.

30 R. Meyer, S. Cogan, T. Nguyen, R. Rauh, *IEEE Trans. Neural. Sys. Rehabil. Eng.* 2001, **9**, 2–10.

31 C. M. Riley, T. M. Rosanske (1996) Development and validation of analytical methods. Elsevier, New York.

32 M. E. Swartz, I. S. Krull (1997) Analytical method development and validation. Marcel Dekker, New York.

33 J. Ermer, M. JHMcB (2005) Method validation in pharmaceutical analysis. Weinheim, Wiley VCH.

34 P. De Bievre, H. Gunzler (2005) Validation in chemical measurements. Springer, Berlin.

35 S.A. Ozkan (2012) Electroanalytical Methods in Pharmaceutical Analysis and Their Validation, HNB Publishing, New York.

36 Council Directive 98/83/EC 1998 on the quality of water intended for human consumption, Official Journal of the European Communities, http://eurlex.europa.eu/LexUriServ/ LexUriServ.do?uri=OJ:L:1998:330:0032:0054:EN:PDF

Fig. 1 Surface characterization. (A) TEM images of IrOx NPs. SEM images of SPCE (B), SPCE/IrOx/GA (C) and SPCE/IrOx/GA/ IrOx-BSA (D). Impedance studies (E) of the modified electrodes surfaces. Left SEM images were taken using backscattered electrons mode. The scale bare of SEM images is 200 nm.

Fig. 2 Current-time responses of SPCE/GA/Tyr-BSA and SPCE/IrOx/GA/Tyr-BSA for the successive addition of 5 µM catechol solution, during stirring conditions within a working potential of -0.2V using 0.1 M phosphate buffer (PB) at pH 6.5 with 0.1 M KCl. Selectivity evaluation for catechol biosensor in present of successive additions of 50 µM aniline, benzaldehyde, benzylalcohol, Mg^{2+}, Ca^{2+}, 5µM of catechol and 25 µM Cu^{2+} (B).

Fig. 3 Schematic representation of proposed detection mechanism, displaying the tyrosinase (Tyr) and reaction involved in the catechol detection at the SPE modified with IrOx NPs (A). Catalytic cycles of the oxidation of catechol to o-quinone over two Cu atoms within the active site of Tyrosinase enzymes (B).

Fig. 4 Typical current–time response curves for the successive additions of different catechol concentration (A); inset: magnification of the initial steps. Biosensor calibration given as current versus catechol concentration (B).

Fig. 5 Effect of substrate amount (A) and incubation time (B) in the residual activity of the catechol biosensor after pesticide incubation.

Fig. 6 Calibration curve of the biosensor as a function of the CPF concentration and the inhibition percentage (A). CPF recovery percentage from PBS, tap water and river water, using catechol biosensor (B).

Fig. 7 IrOx Nanoparticles induced dual catalytic/inhibition based detection of catechol (A) and CPF (B) using the same platform.
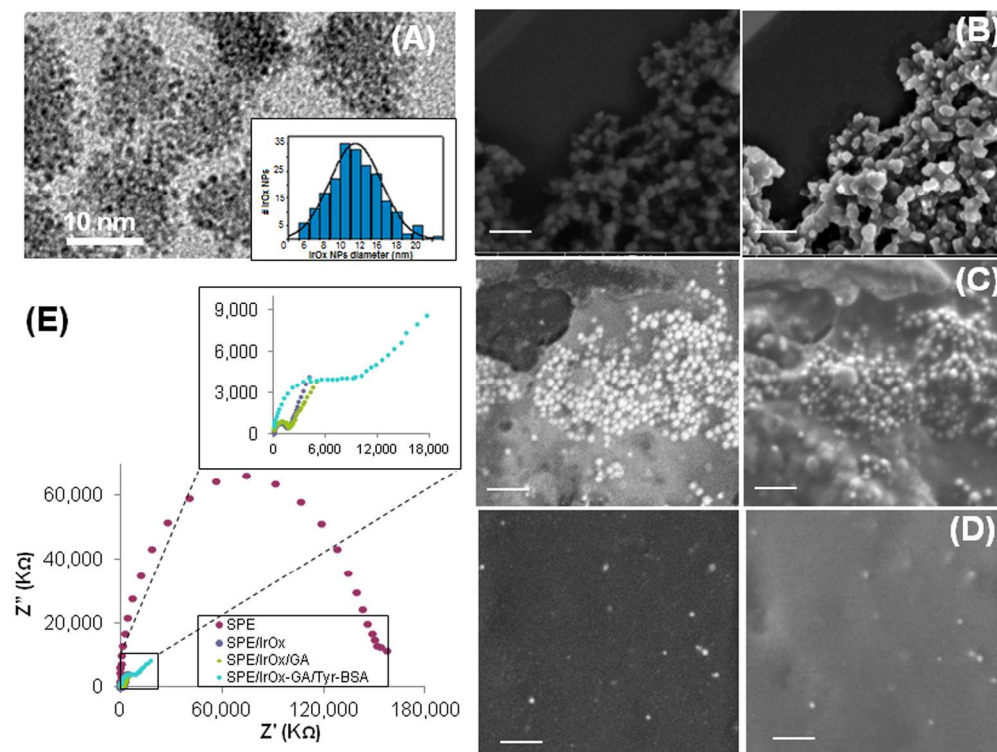
Fig. 1 Surface characterization. (A) TEM images of IrOx NPs. SEM images of SPCE (B), SPCE/IrOx/GA (C) and SPCE/IrOx/GA/ IrOx-BSA (D). Impedance studies (E) of the modified electrodes surfaces. Left SEM images were taken using backscattered electrons mode. The scale bare of SEM images is 200 nm.
164x124mm (300 x 300 DPI)
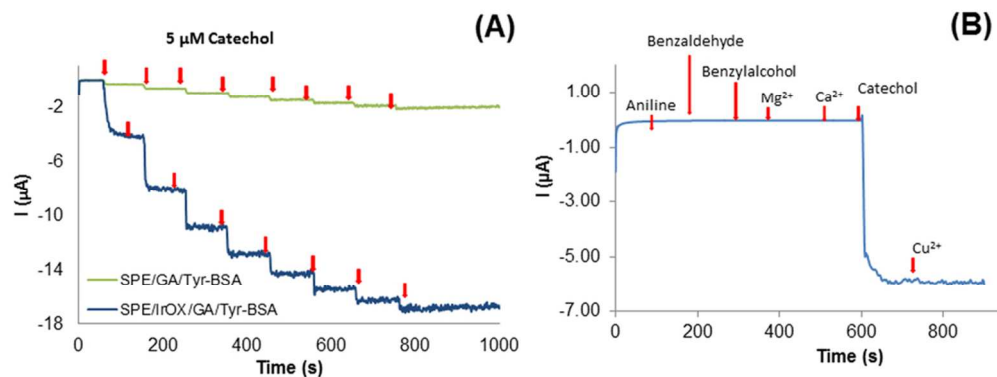
Fig. 2 Current-time responses of SPCE/GA/Tyr-BSA and SPCE/IrOx/GA/Tyr-BSA for the successive addition of 5 µM catechol solution, during stirring conditions within a working potential of -0.2V using 0.1 M phosphate buffer (PB) at pH 6.5 with 0.1 M KCl. Selectivity evaluation for catechol biosensor in present of successive additions of 50 µM aniline, benzaldehyde, benzylalcohol, Mg2+, Ca2+, 5µM of catechol and 25 µM Cu2+ (B).
90x34mm (300 x 300 DPI)
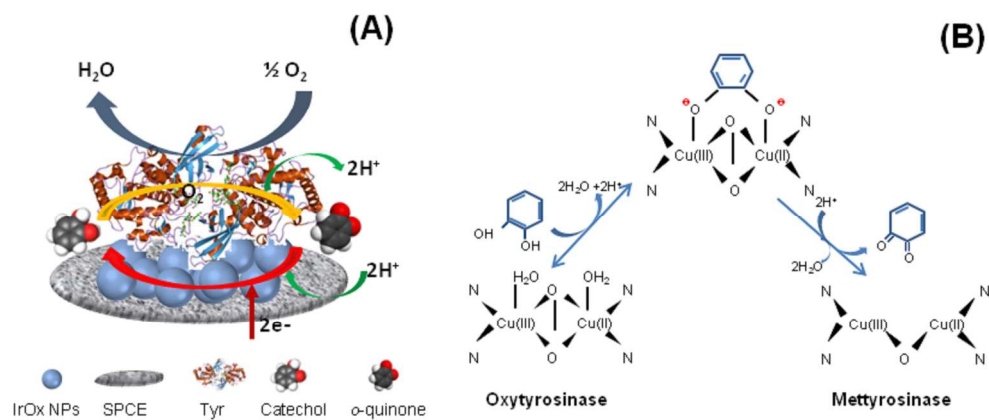
Fig. 3 Schematic representation of proposed detection mechanism, displaying the tyrosinase (Tyr) and reaction involved in the catechol detection at the SPE modified with IrOx NPs (A). Catalytic cycles of the oxidation of catechol to o-quinone over two Cu atoms within the active site of Tyrosinase enzymes (B).
1322x561mm (96 x 96 DPI)
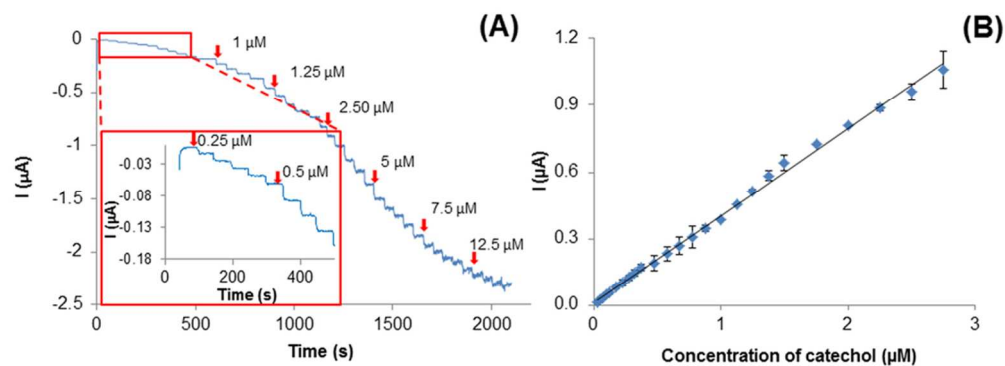
Fig. 4 Typical current–time response curves for the successive additions of different catechol concentration (A); inset: magnification of the initial steps. Biosensor calibration given as current versus catechol concentration (B).
89x32mm (300 x 300 DPI)
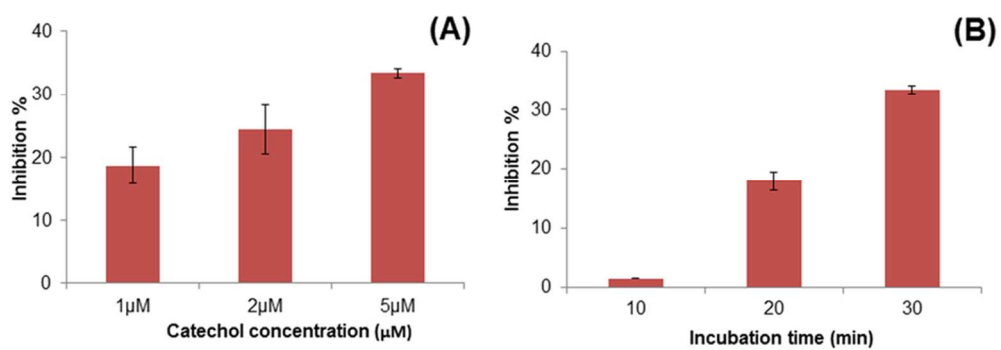
Fig. 5 Effect of substrate amount (A) and incubation time (B) in the residual activity of the catechol biosensor after pesticide incubation.
79x27mm (300 x 300 DPI)
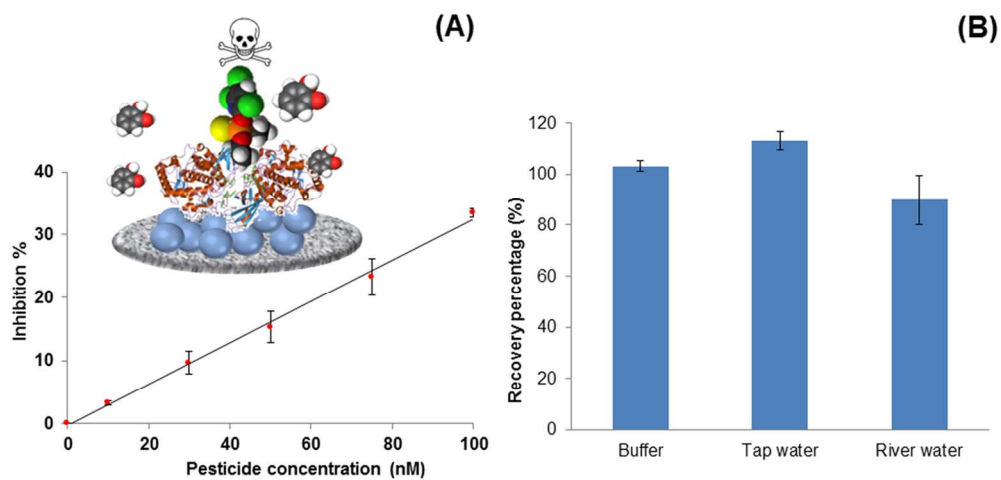
Fig. 6 Calibration curve of the biosensor as a function of the CPF concentration and the inhibition percentage (A). CPF recovery percentage from PBS, tap water and river water, using catechol biosensor (B).
117x56mm (300 x 300 DPI)
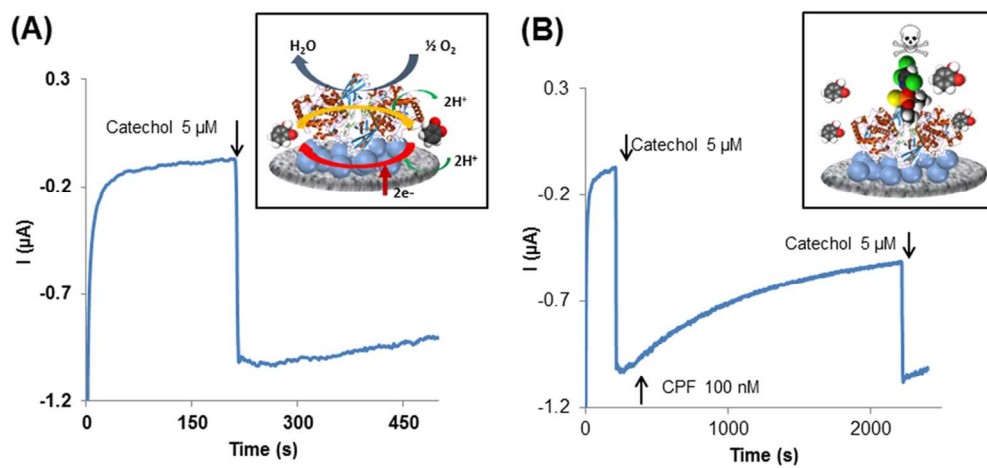
Fig. 7 IrOx Nanoparticles induced dual catalytic/inhibition based detection of catechol (A) and CPF (B) using the same platform.
106x48mm (300 x 300 DPI)

A table of contents entry
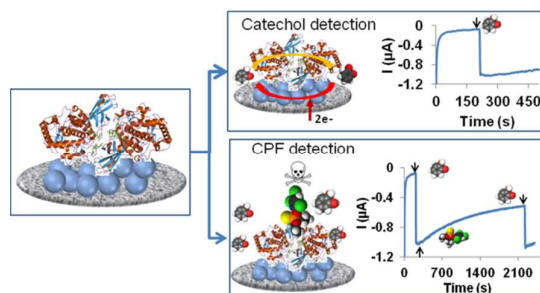
Tyrosinase biosensor based on iridium oxide nanoparticles for induced dual catalytic/inhibition for detection of phenol and pesticide